Progress in Natural Science: Materials International 2012;22(2):169–174

Chinese Materials Research Society

Progress in Natural Science: Materials International

www.elsevier.com/locate/pnsmi
www.sciencedirect.com

ORIGINAL RESEARCH

Corrosion behavior of Mg–Y alloy in NaCl aqueous solution

Xin Zhang[a,b,c,*], Kui Zhang[a], Xia Deng[a], Hongwei Li[b,c], Yongjun Li[a], Minglong Ma[a], Ning Li[b,c], Yanlong Wang[b,c]

[a]*State Key Laboratory for Fabrication and Processing of Nonferrous Metals, Beijing General Research Institute for Nonferrous Metals, Beijing 100088, China*
[b]*Beijing Engineering Research Center for Advanced Manufacturing and Evaluation of Special Vehicle Parts, Beijing 100072, China*
[c]*Center of Technology, Beijing North Vehicle Group Corporation, Beijing 100072, China*

Received 30 November 2011; accepted 2 March 2012
Available online 15 April 2012

KEYWORDS
Mg–Y;
Corrosion;
Microstructure

Abstract The corrosion behavior of Mg–(0.25, 2.5, 5, 8 and 15)Y alloys in 3.5wt.% NaCl aqueous solution was investigated. It was found that the degree of corrosion deterioration increased with increasing immersion time up to 2 h. Corrosion modes for the alloys with low and high content of Y element were general corrosion and pitting corrosion, respectively, and the threshold content for the corrosion mode change was 2.5% for the tested alloys. The experimental results showed that the addition of Y refined the grain of the alloy, and the distribution, i.e., continuous or not, of the $Mg_{24}Y_5$ phases had great effect on the corrosion rate and corrosion mode.

1. Introduction

Owing to the high specific strength, high damping capacity, excellent machinability, good electromagnetic shielding characteristics and easy recyclability, the magnesium alloys are attractive for various engineering applications [1]. They may complement and even compete with other structural materials, such as, aluminum and its alloys, stainless steels in a large range of applications if some surface properties can be improved [2]. However, poor resistance to corrosion of the magnesium alloys has restricted their widespread use in many engineering industries. It is well known that the addition of rare earth (RE) elements is an effective way to have a beneficial effect on the corrosion resistance of magnesium alloys, which has mainly been attributed to the formation of metastable RE-containing phases along the grain boundaries and the other reasons including purification of the melt, and so on [3–7]. It has been found that the addition of yttrium can improve the corrosion resistance of the magnesium and has been used in several commercially available alloys, and therefore yttrium is selected as the alloying element in the magnesium alloys.

In this work the rare earth Y was used to act as the alloying element in an attempt to promote the formation of a Mg–Y surface system with enhanced corrosion resistance, in

*Correspondence to: Branch Box 304, Box 968, Beijing 100072, China. Tel.: +86 10 83807347.
E-mail address: bjzx201@yahoo.com.cn (X. Zhang).

Peer review under the responsibility of Chinese Materials Research Society.
http://dx.doi.org/10.1016/j.pnsc.2012.03.014

Production and hosting by Elsevier

particular under NaCl conditions. It was also the aim of this work to contribute to the study of the influence and role of the rare earth Y in the corrosion progress and mechanisms.

2. Experimental

Magnesium–yttrium alloys were prepared in a crucible furnace under the shelter of CO_2+SF_6 gases and cast in a water cooled metallic model. The actual compositions of magnesium alloys were presented in Table 1. The Mg–Y alloy was cut into samples with dimensions of 10 mm × 10 mm × 10 mm.

The alloys were investigated by X-ray diffraction. The samples were wet ground through successive grades of silicon carbide abrasive papers from P120 to P1500. The etching reagent 5 ml HNO_3+95 ml ethanol was used to reveal the constituents and microstructure of Mg–(0.25, 2.5, 5, 8 and 15)Y alloys. The corrosion products were cleaned by dipping in a 400 ml aqueous solution of 10% CrO_3+1% $AgNO_3$ in boiling condition for 4–6 min. Corrosion morphologies of the alloys were observed by JSM-6510A analytical scanning electron microscope.

The electrochemical characteristics of Mg–Y alloys were investigated through a Autolab potentiostat/Galvanostat Model 273A coupled with HF Frequency Response Analyzer SI1255 in the neutral 3.5% NaCl solution. The polarization measurements and the open circuit potentials were carried out at a scan rate of 0.5 mV/s, from −100 mV to +400 mV with respect to the corrosion potential (E_{corr}). EIS measurements were conducted with a perturbing signal of AC amplitude of 5 mV and a frequency ranging from l00 Hz to 5 mHz.

Table 1 Nominal composition of the materials tested.

Series	Material	Chemical composition (wt%)	
		Y	Mg
1	Mg–0.25Y	0.24	Bal
2	Mg–2.5Y	2.08	Bal
3	Mg–5Y	5.23	Bal
4	Mg–8Y	7.46	Bal
5	Mg–15Y	13.78	Bal

3. Results and discussion

3.1. Microstructure of Mg–Y alloys

Fig. 1 showed the optical microstructures of the as-cast Mg–(0.25, 2.5, 5, 8 and 15)Y alloys. As for the Mg–(0.25, 2.5)Y

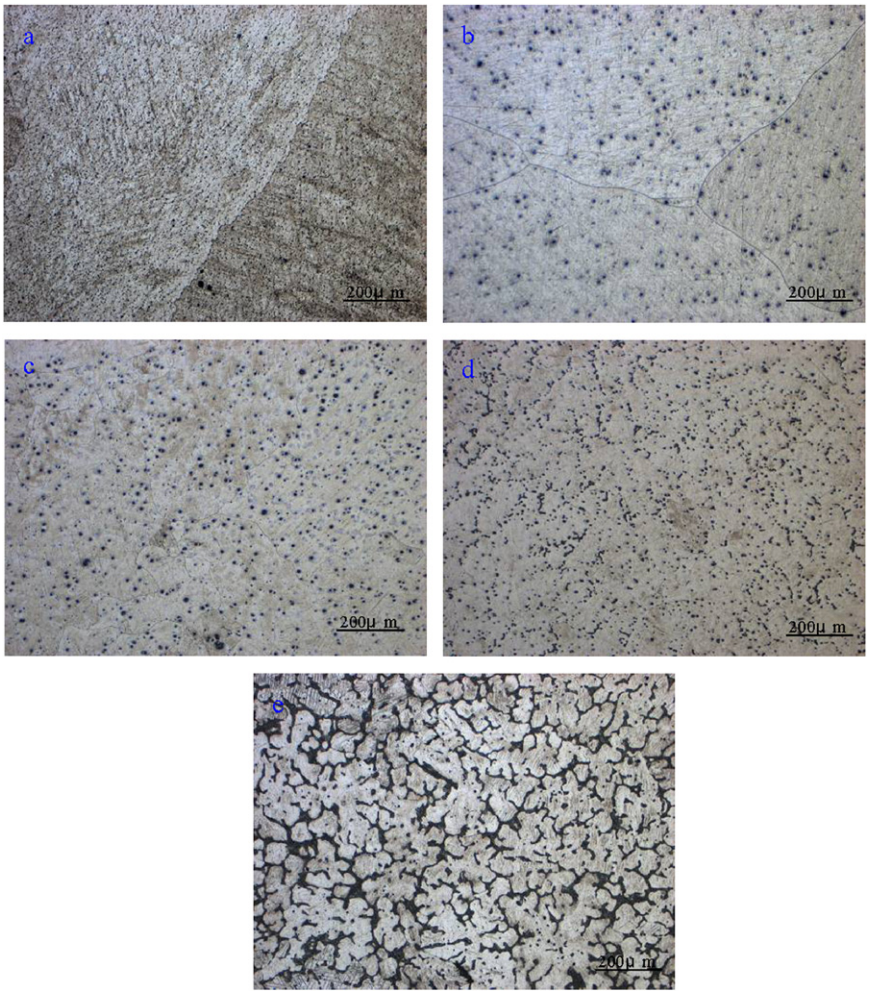

Fig. 1 Microstructures spectrum of specimens: (a) Mg–0.25Y; (b) Mg–2.5Y; (c) Mg–5Y; (d) Mg–8Y; (e) Mg–15Y, magnification, × 50.

alloys, the element Y was dissolved into the α-Mg phase absolutely, and the α-Mg was only seen from the microstructures. However, it could be seen that the microstructure of the alloy consisted of the primary α-Mg phase and the second phases according to the magnesium–yttrium phase diagrams and the solidification mechanism of metal for Mg–(5, 8 and 15)Y alloys. The yttrium element gathered to form the network structures distributed along the grain boundaries, as shown in Fig. 1(c, d, e), and some eutectic phases also located in the grain interiors. It was obvious that the dimension of the grain decreased with increasing of Y addition for the as-cast Mg–(0.25, 2.5, 5, 8 and 15)Y alloys.

The Y and Mg were both the structure of the hexagonal close packed lattice, and the parameters of the structure were expressed as $\alpha_{Mg} = 0.323 \times 10^{-9}$ m, $c_{Mg} = 0.520 \times 10^{-9}$ m, $\alpha_Y = 0.365 \times 10^{-9}$ m and $c_Y = 0.573 \times 10^{-9}$ m. The diameters of Y and Mg were as following: $R_{Mg} = 1.6 \times 10^{-10}$ m, $R_Y = 1.82 \times 10^{-10}$ m [8]. According to the coherent crystal lattice theory, in the heterogeneous nucleation process, the bottom lattice face always tries to combine with a most suitable crystal lattice phase to form a minimum interface of σ_{cs}. So the structure of Y had the similar crystal lattice to that of magnesium, and the difference of atomic radius was very little, so the Y could be used as the crystal core of the α-Mg phase. A large number of Y atoms greatly improved the nucleation rate of the α-Mg phases; the grain of the α-Mg phases were not easy to grow, so the Y had the great refinement effect on the magnesium alloy.

According to the XRD spectrum showed in Fig. 2, the microstructure view clearly showed that the eutectic phases were the α-Mg phases for the Mg–(0.25, 2.5)Y alloys and the eutectic consisted of large $Mg_{24}Y_5$ phase particles and the eutectic α-Mg phase for the Mg–(5, 8 and 15)Y alloys. These $Mg_{24}Y_5$ particles formed in cast alloy as a result of incomplete

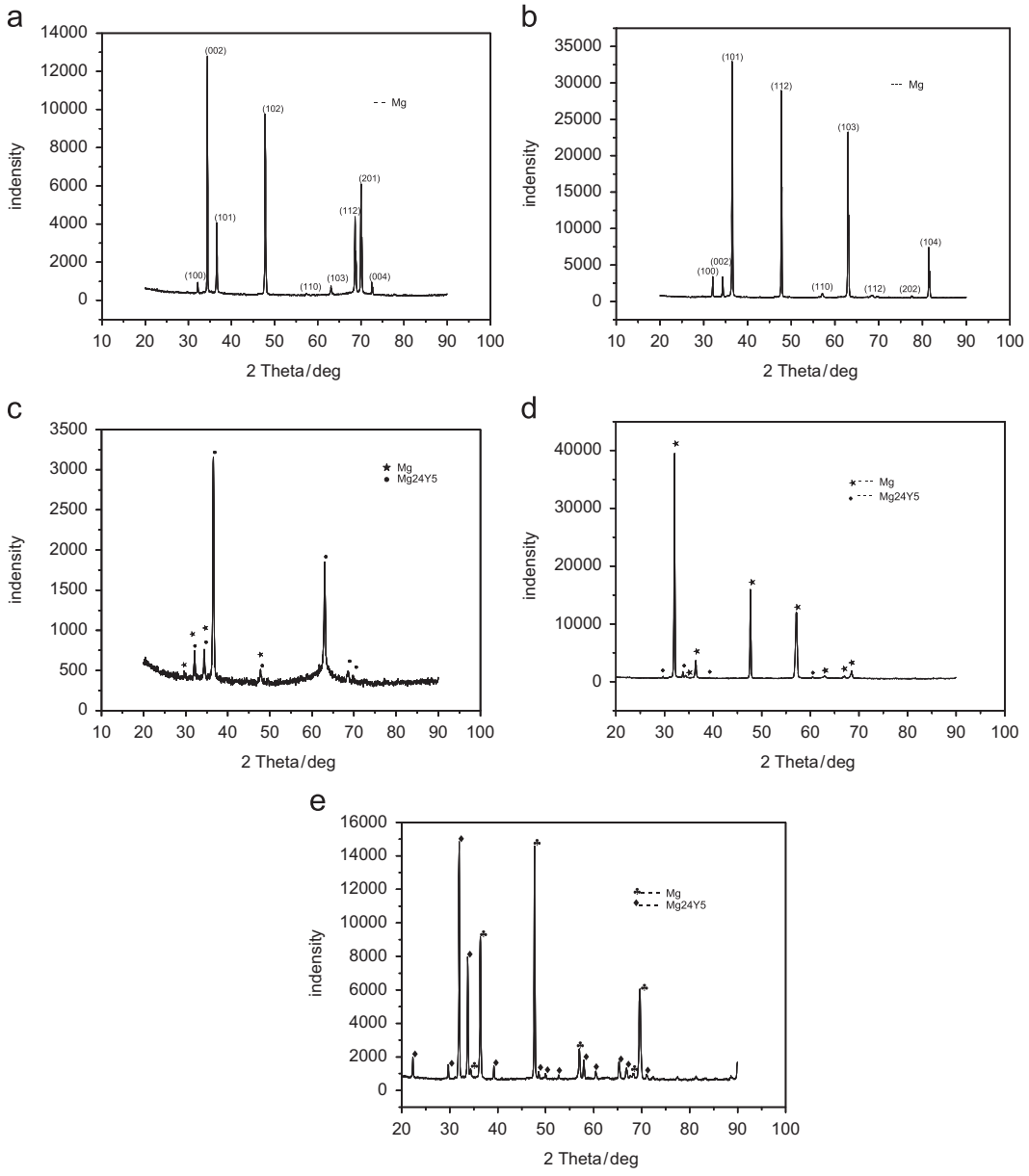

Fig. 2 XRD spectrum of specimens: (a) Mg–0.25Y; (b) Mg–2.5Y; (c) Mg–5Y; (d) Mg–8Y; (e) Mg–15Y.

dissolution of the second phase arranged over grain boundaries in the form of continuous chains.

3.2. Corrosion potential

Fig. 3 showed the corrosion potentials of the Mg–(0.25, 2.5, 5, 8 and 15)Y alloys with time immersed in 3.5% NaCl solution. The results in Fig. 3 showed that the corrosion potentials of Mg–Y alloys increased with the addition of yttrium, up to 2.5%, while the corrosion potentials decreased when the addition of yttrium was above 2.5% due to the formation of the second phases. From Fig. 3, it has been found that: (1) The corrosion potential of the Mg–(8 and 15)Y alloys kept steady and nearly constant during most of the immersion time. (2) The corrosion potential of the Mg–(0.25 and 5)Y alloys increased with the increment of immersion time up to about 1000 s, and the corrosion potential kept rapidly moving up and down at −1.6075 V and −1.5525 V during the remaining period of immersion time of about 1000 s. (3) The corrosion potential of Mg–2.5%Y increased to the highest one quickly in the initial several seconds as soon as they were immersed into the solution, then decreased quickly. After reaching the low values after about 1500 s, the curves of the sample got up slightly with little fluctuation. The value of the open circuit potential kept rapidly moving up and down at −1.5499 V during the remaining period of immersion time about 300 s.

3.3. Polarization curves

Fig. 4 showed the potentiodynamic polarization curves for Mg–(0.25, 2.5, 5, 8 and 15)Y specimens in 3.5% NaCl solution. The corrosion properties derived from these experimental data were presented in Table 2. All the specimens showed passivity in the solution; the current density decreased quickly when the films formed on the surface broke down.

Judging from the cathodic branches, the addition of Y obviously activated the cathodic reaction. However, the influence of Y on the anodic reaction was not as obvious as that on the cathodic reaction. And the anodic branch presented an obvious step with increasing of Y addition, which indicated that the rare earth element Y could increase the stability of the corrosion film on the sample surface.

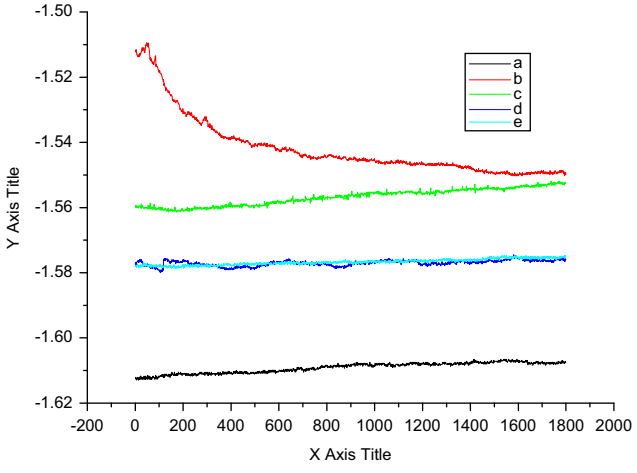

Fig. 3 Corrosion potential of specimens in 3.5% NaCl solution: (a) Mg–0.25Y; (b) Mg–2.5Y; (c) Mg–5Y; (d) Mg–8Y; (e) Mg–15Y.

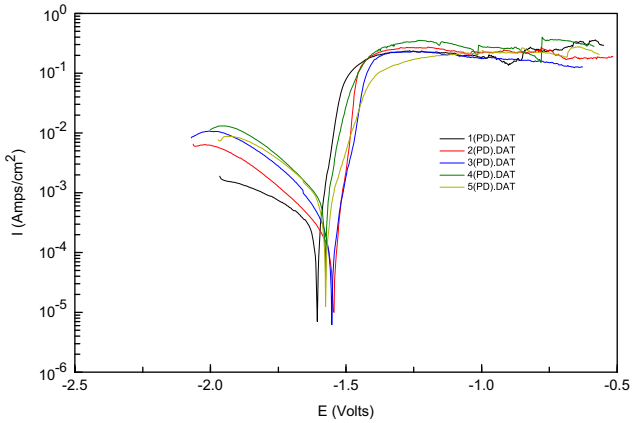

Fig. 4 Polarization curves of specimens in 3.5% NaCl solution: (1) Mg–0.25Y; (2) Mg–2.5Y; (3) Mg–5Y; (4) Mg–8Y; (5) Mg–15Y.

Table 2 Electrochemical corrosion data for Mg–(0.25, 2.5, 5, 8 and 15)Y specimens in 3.5% NaCl solution.

Specimens	E_{corr} (V)	I_{corr} (Amp/cm^2)	E_{pit} (V)
Mg–0.25Y	−1.6075	0.00025098	−1.6097
Mg–2.5Y	−1.5499	0.00007698	−1.5599
Mg–5Y	−1.5525	0.00015639	−1.5625
Mg–8Y	−1.576	0.00011608	−1.583
Mg–15Y	−1.575	0.00015981	−1.581

Consequently, the corrosion resistance of the magnesium–yttrium alloys was improved in virtue of the addition of Y.

It could be found that the cathodic sides of magnesium–yttrium were driven with hydrogen evolution reaction. The corrosion current density gradually decreased with moving the potential toward E_{corr}, implying that the hydrogen evolution rate diminished. After the potential reached E_{corr}, the curves entered into the anodic region. The corrosion current density increased slowly with increasing of anodic potential. When the corrosion potential reached a certain value, the pitting corrosion occurred. Once the anodic potential reached the corrosion potential of the film breakdown, the surface oxide film fractured and the magnesium substrate corroded quickly [9]. The onset of pitting was not visible in Fig. 4, since pitting potential (E_{pit}) is very close to E_{corr}. Consequently, it should be expected that these alloys suffer pitting attack immediately after their immersion in the aggressive media at the open circuit potential. However, the current densities of the cathodic branch and, therefore, the growth of corrosion products on the material surface were quite high, suggesting general corrosion attack as the main mechanism of degradation [10].

3.4. Electrochemical impedance spectroscopic

The Electrochemical Impedance Spectroscopic(EIS) measurements at the open circuit potential of Mg–(0.25, 2.5, 5, 8 and 15)Y specimens after exposing in 3.5% NaCl solution were shown in Fig. 5. From Fig. 5, the capacitive loops shrinked and the charge transfer resistance reduced in the solution, while

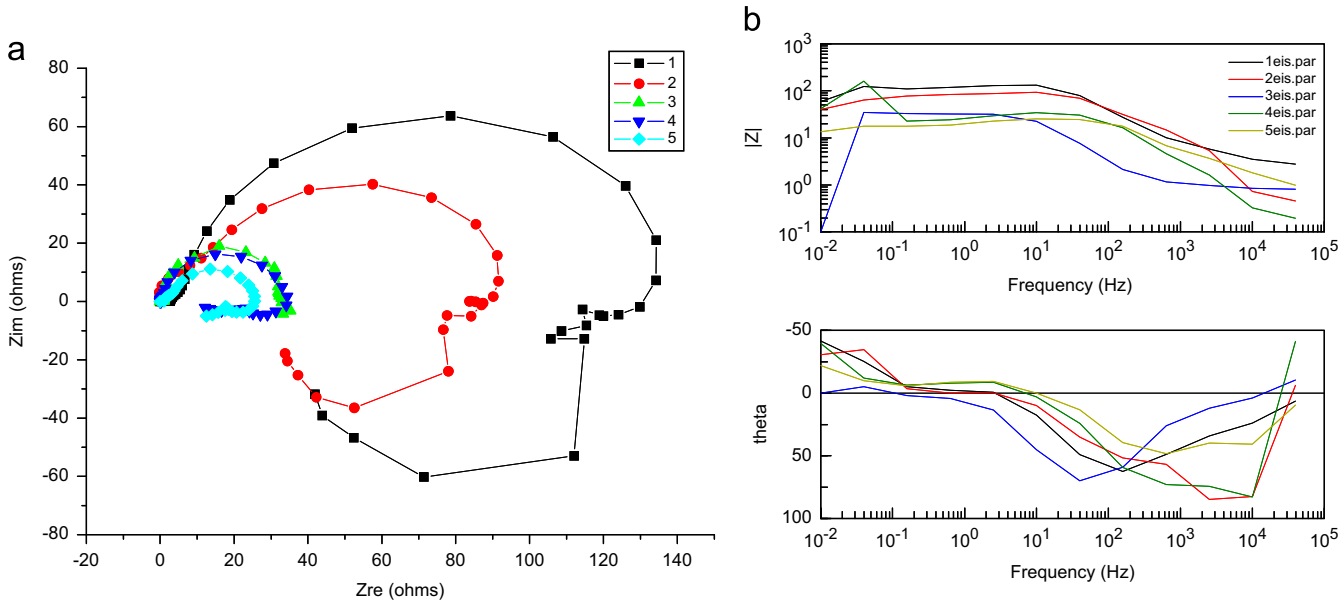

Fig. 5 Electrochemical Impedance Spectroscopic (EIS) of specimens in 3.5% NaCl solution: (a) Nyquist plots; (b)Bode plots (1) Mg–0.25Y; (2) Mg–2.5Y; (3) Mg–5Y; (4) Mg–8Y; (5) Mg–15Y.

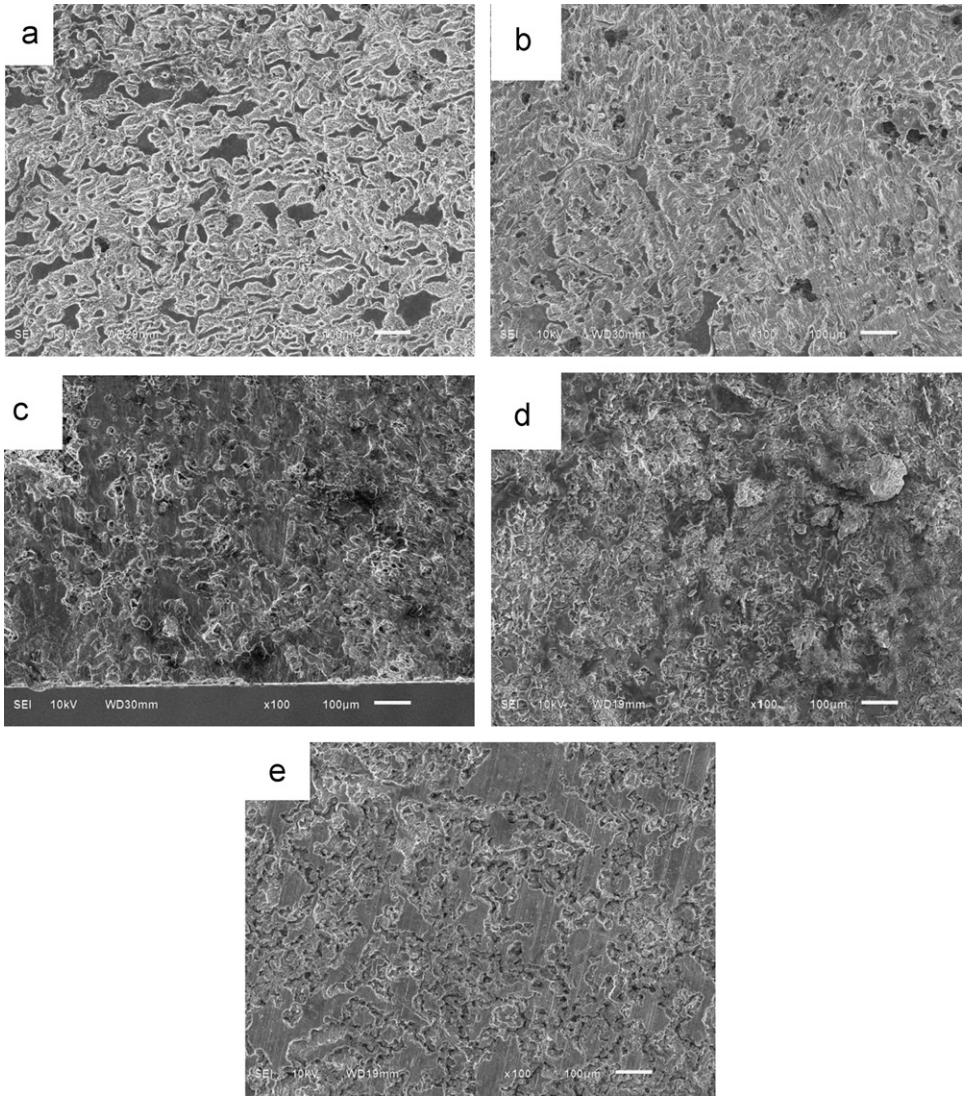

Fig. 6 Corrosion morphologies of specimens: (a) Mg–0.25Y; (b) Mg–2.5Y; (c) Mg–5Y; (d) Mg–8Y; (e) Mg–15Y.

corrosion resistant decreased. The Nyquist plot for all the samples without immersion treatment included three well-defined loops, one high frequency capacitive loop, one medium frequency capacitive loop and one short low frequency inductive loop. Large capacity loop represented the charge transfer resistance of an actively corroding electrode, with determined capacitance values consistent with the electrochemical double layer. High frequency capacitive loop was attributed to the charge transfer reaction in the electric double layer formed at the interface between metal surface and corrosive medium. The polarization curve result of the tested samples could prove the film existed on the surface on Mg–Y alloys. The low frequency inductive loop was attributed to the corrosion nucleation at the initiation stage of pitting corrosion [11]. With increasing the immersion time, the hydrogen evolution procedure resulted into the occurrence of the pitting corrosion.

3.5. *Corrosion morphology*

The corrosion morphologies of the tested materials after immersing for 2 h in 3.5% NaCl solution are shown in Fig. 6 in which the corrosion products were removed. From the corrosion micrographs, the corrosion mechanism of Mg–(0.25, 2.5)Y was general corrosion since the Y element dissolve into the α-Mg, and the corrosion potential of the every spot on surface almost have the same value. When the Y addition increased to above 2.5%, the second phase $Mg_{24}Y_5$ was formed on the grain boundary. The second phase $Mg_{24}Y_5$ was highly anodic to the α-Mg phase and could thus act as an effective anode to cause the galvanic corrosion. And therefore the corrosion mode was pitting corrosion. It has been observed that for the Mg–15Y alloy, the degree of corrosion was obviously lighter than Mg–(5, 8)Y alloys since the amount of second phase $Mg_{24}Y_5$ exceeds a certain value and forms a continuous barrier to prevent the corrosion, and the corrosion presented in the area with the less $Mg_{24}Y_5$ phase [12]. Therefore the pitting corrosion of Mg–15Y alloy was more obvious than that of other studied alloys.

Pitting corrosion was a typical corrosion mode to the dual-phase magnesium alloy because the corrosion potential difference could accelerate the corrosion rate of the low corrosion potential phase. Thus, the micro-galvanic corrosion led to the nucleation of corrosion pits on the α-Mg phase. Corrosion pits initiated on the bare α phase of the samples immersed in 3.5% NaCl aqueous solution in the initial corrosion, and also turned into the main corrosion mode judging from the corrosion morphology [13]. After the nucleation, corrosion pits continuously extend along the alloy surface while they develop in the direction perpendicular to the alloy surface. In addition, Cl^- was a harmful ion to magnesium alloy [14]. Chen et al. [15] reported that Cl^- could accelerate the corrosion of magnesium alloy, which may be attributed to the fact that Cl^- could get across the oxide and hydroxide films and reach the corrosion interface in the aqueous solution.

As for the pitting corrosion, the size and depth of the samples increased with the increasing Y content, and the corrosion pits nucleate on the α-phase and propagate continuously with increasing Y content. In fact, the second phase $Mg_{24}Y_5$ was an important obstacle to the propagation of corrosion pits, the more the second phase $Mg_{24}Y_5$ was isolated, the more the corrosion pit easily developed into the alloy matrix. Consequently, the refinement of the second phase $Mg_{24}Y_5$ played a negative role in suppressing the propagation of corrosion pits into the alloy matrix [16].

4. Conclusions

1) Mg–Y alloys with the addition of Y element less than 2.5% heterogeneously corroded in the 3.5% NaCl solution, while Mg–Y alloys with the addition of Y element more than 2.5% corroded with the mode of pitting corrosion for the studied alloys.
2) Corrosion pits initiated on the bare α-phase of the samples immersed in 3.5% NaCl aqueous solution.
3) The addition of Y element refined the grain size of Mg–Y alloy, and promoted the formation of the second phase $Mg_{24}Y_5$ which acted as the anode to accelerate the corrosion, however the $Mg_{24}Y_5$ phase could also suppress the propagation of corrosion pits when the addition of Y element was excess a certain amount.
4) The presence of Cl^- ions resulted in the breakdown of the film formed on the surface deposit and thereby prompted pit formation.

Acknowledgments

The authors wished to acknowledge the financial support of the National Key Technology R&D Program of China (nos. 2011BAE22B01 and 2011BAE22B06). This work was also supported by Beijing Engineering Research Center for Advanced Manufacturing and Evaluation of Special Vehicle Parts.

References

[1] X. Cao, M. Jahazi, J.P. Immarigeon, W. Wallace, Journal of Materials Processing Technology 171 (2006) 188.
[2] A.H. Cotrell, Edward Arnold Publications, London (1975), pp. 156.
[3] Xing-Wu Guo, Jian-Wei Chang, Shang-Ming He, Wen-Jiang Ding, Xishu Wang, Electrochimica Acta 52 (2007) 2570.
[4] M.X. Zhang, P.M. Kelly, Scripta Materialia 48 (2003) 379.
[5] Ming Liu, Patrik Schmutz, Peter J. Uggowitzer, Guangling Song, Andrej Atrens, Corrosion Science (52) (2010) 3687.
[6] Ryan C. Wolfe, Barbara A. Shaw, Journal of Alloys and Compounds 437 (2007) 157.
[7] Xin Zhang, Kui Zhang, Xinggang Li, Cong Wang, Hongwei Li, Changshun Wang, Xia Deng, Progress in Natural Science: Materials International 21 (2011) 314.
[8] R.W. Chan, in: Physical Metallurgy, Fourth ed., North Holland, New York, 1996 (February 1).
[9] Y.W. Song, D.Y. Shan, R.S. Chen, E.H. Han, Corrosion Science 51 (2009) 1087.
[10] A. Pardo, M.C. Merino, A.E. Coy, R. Arrabal, F. Viejo, E. Matykina, Corrosion Science 50 (2008) 823.
[11] Yong Wang, Mei Wei, Jiacheng Gao, Jinzhu Hu, Yan Zhang, Materials Letters 62 (2008) 2181.
[12] Wei Zhou, Tian Shen, Naing Naing Aung, Corrosion Science 52 (2010) 1035.
[13] S. Amira, D. Dubé, R. Tremblay, E. Ghali, Materials Characterization 59 (2010) 1508.
[14] T. Zhang, Y. Li, F.H. Wang, Corrosion Science 48 (2006) 1249.
[15] J. Chen, J.Q. Wang, E.H. Han, Junhua Dong, Wei Ke, Electrochim Acta 52 (2007) 3299.
[16] A.D. Sudholz, K. Gusieva, X.B. Chen, B.C. Muddle, Corrosion Science 53 (2011) 2277.